1995ApJ...452..599L

THE ASTROPHYSICAL JOURNAL, 452:599–604, 1995 October 20
© 1995. The American Astronomical Society. All rights reserved. Printed in U.S.A.

NEAR-INFRARED SPECTROSCOPY OF THE ARP 220 NUCLEI: MEASURING THE NUCLEAR ROTATION

J. E. LARKIN, L. ARMUS, R. A. KNOP, K. MATTHEWS, AND B. T. SOIFER
Palomar Observatory, California Institute of Technology, 320-47, Pasadena, CA 91125
Received 1995 September 22; accepted 1995 May 2

ABSTRACT

We report spatially resolved near-infrared spectroscopy at a resolution $(\lambda/\Delta\lambda) \sim 1000$ of the double nucleus of Arp 220 in the Paβ, Brγ, [Fe II] ($\lambda = 1.2567$ μm), and H_2 (1–0 $S1$) ($\lambda = 2.1218$ μm) emission lines. The Brγ hydrogen recombination line is strongly peaked on the two nuclei, and the Paβ is centered on the western nucleus with emission across the eastern nucleus. Both lines show a velocity separation of $\sim$200 km s^{-1} between the eastern and western nuclei, the former being redshifted relative to the latter. Both the magnitude and the direction of this velocity shift are consistent with recent CO millimeter measurements of larger scale gas motions over the central 2″. The implied rotation requires a central mass greater than 1.5×10^9 $M_\odot$. The extinction determined from the ratio of the Paβ and Brγ lines is found to be $A_V \sim 10$ mag for the western nucleus and $A_V \sim 13$ mag for the eastern nucleus. The [Fe II] and H_2 lines show a different morphology than the hydrogen recombination lines, particularly the H_2 line which shows significant flux between the two nuclei. The [Fe II] and H_2 lines also do not show velocity splitting between the two nuclei. The difference in spatial and velocity structure between the [Fe II], H_2, and ionized hydrogen lines implies multiple excitation processes are at work within the nucleus. The [Fe II] and H_2 lines may have a significant contribution from extranuclear shocks related to either a starburst-driven wind or the ongoing merger process.

Subject headings: galaxies: individual (Arp 220) — galaxies: kinematics and dynamics — galaxies: nuclei — infrared: galaxies

1. INTRODUCTION

Arp 220 (=IC 4553/4 = UGC 9913 = IRAS 15327+2340) is the nearest ($cz \sim 5450$ km s^{-1}) and therefore the most studied example of an ultraluminous infrared galaxy (ULIRG), with a far-infrared luminosity of 1.5×10^{12} $L_\odot$ (Sanders et al. 1988). ULIRGs, which were defined as a class to have infrared luminosities, L (8–1000 μm), greater than 10^{12} $L_\odot$ by Soifer et al. (1987) and Sanders et al. (1988), are thought to be the result of the recent collision and subsequent merging of two gas-rich galaxies (Sanders et al. 1988). In these galaxies, most of the energy emerges in the far-infrared.

In the visual, Arp 220 possesses two faint tidal tails (e.g., Joseph & Wright 1985) and two bright knots straddling a thick dust lane that obscures the true nuclei (e.g., Joy et al. 1986). At 2.2 μm, a double nucleus was found by Graham et al. (1990) with a spatial separation of 0.″95 ± 0.″01 and a position angle of 92°. This separation agrees very well with the 0.″93 separation for the compact, nonthermal, double radio source observed at 6 cm, 2 cm, and 1.3 cm (Becklin & Wynn-Williams 1987; Norris 1988). For $H_0 = 75$ km s^{-1} Mpc^{-1} (which we use throughout this paper), 0.″95 corresponds to a projected separation of only 330 pc. Graham et al. (1990) use this extremely small separation to argue that Arp 220 is in the final stages of a merger.

We present near infrared spectra of Arp 220 that reveal two components of H^+ gas coincident with the two infrared nuclei that are clearly separated in both position and velocity space. Also presented are observations of molecular and forbidden line transitions of H_2 and [Fe II] that do not show the same spatial and velocity structures as the hydrogen recombination lines. These spectra have a spectral resolution a factor of 10 greater than any previously published near-infrared emission-line spectra over the centralmost region of Arp 220 and were taken under excellent seeing conditions.

2. OBSERVATIONS AND DATA REDUCTION

Near-infrared spectra of Arp 220 were obtained using the 200 inch (5 m) Hale telescope at Palomar Observatory on 1994 July 26. The spectra were taken with a new near-infrared long-slit spectrometer, fully described in Larkin et al. (1995). The spectrometer is cryogenically cooled and can take direct images through the same optical path by placing a flip mirror in front of the grating. The spectrometer uses a separate near-infrared camera containing a 256 × 256 NICMOS 3 HgCdTe detector. At the f/70 Cassegrain focus, the array has a plate scale of 0.″167 pixel^{-1} along the spatial axis or along both axes in the imaging mode. Two gratings are available with $\sim$1000 and $\sim$4000 resolution for a 0.″7 slit width.

During these observations, the seeing, as determined from images of a calibrator star, was $\sim$0.″5 at 2 μm, although the observations of Arp 220 may have a slightly worse resolution since we cannot fully resolve the separate K-band nuclei in images taken with the spectra. The sky had very light cirrus clouds, which made for nonphotometric conditions. A nearby star was used with an offset guider which controls a tip-tilt secondary. With this guiding system, tracking errors (<0.″1) are insignificant compared to the seeing.

For the Arp 220 observations, the lower resolution grating was used with the slit set at 0.″75 × 40″. The slit was oriented east-west so that the two nuclei, which have a position angle of 92° (Graham et al. 1990), could both be included in the same spectrum. Two grating angles were used to give wavelength coverages from 1.240 to 1.295 μm ($R \sim 1050$, FWHM $\sim$ 280 km s^{-1}) and 2.090 to 2.200 μm ($R \sim 800$, FWHM $\sim$ 375 km s^{-1}). These wavelength ranges were selected to include the redshifted [Fe II] ($\lambda = 1.2567$ μm), and Paβ ($\lambda = 1.2818$ μm) spectral lines and the redshifted H_2 ($\lambda = 2.1213$ μm) and Brγ ($\lambda = 2.1655$ μm) lines. All wavelengths quoted in this paper are values in air. The J-band spectrum consisted of two 600 s

© American Astronomical Society • Provided by the NASA Astrophysics Data System

1995ApJ...452..599L

exposures in which the nucelus was moved 20″ along the slit between the two exposures. The air mass during these exposures was between 1.50 and 1.62. The *K*-band spectrum consisted of four 300 s frames, again with the nucleus moved 20″ back and forth along the slit between frames. The air mass for the *K*-band frames ranged from 1.66 to 1.81. Thus the total integration time was 1200 s for each grating rotation. The Yale Bright Star, BS 5213 (Hoffleit 1964) (spectral type G3 V), was observed at air masses ranging from 1.62 to 1.67 in order to remove telluric absorption features of the atmosphere and as a spectral flat field. No emission or absorption lines other than atmospheric lines were observed in the standard star, although our ability to independently flat-field our spectral flats is limited.

The spectra were reduced by first subtracting image pairs and then dividing by a sky-subtracted standard star frame. Bad pixels were then removed with linear interpolation. Atmospheric OH emission lines in the stellar spectrum were fitted with third-order polynomials in order to remove a slight curvature in the spectral lines and to wavelength-calibrate the spectra. Wavelengths for the OH lines were obtained from Oliva & Origlia (1992). The absolute wavelength calibration is accurate to about 1 pixel (70 km s^{-1}), and the relative wavelength calibration is accurate to about one-third of a pixel (25 km s^{-1}). Slight spatial curvature was removed by fitting spectra taken of a calibrator star that was moved in 5″ steps along the slit. Continuum subtraction was performed by fitting the continuum with a second-order polynomial along every column and subtracting this fit. After continuum subtraction, all features which are unaccounted for are below 3 σ per resolution element.

Broadband 1.25 μm (*J*-band) and 2.2 μm (*K*-band) images were also taken in order to flux-calibrate the spectra. A 5″ synthetic aperture was used to determine the broad band flux calibration from earlier single-beam photometry measurements by Neugebauer et al. (1987). A 0.″75 × 5″ synthetic aperture on the same broadband images was then used to determine the flux within our slit. This was then compared to the spectra that were assumed to be flat across each band (lower resolution grism spectra show that this is a good approximation).

3. RESULTS

3.1. *Hydrogen Recombination Lines*

Figure 1 shows the position-velocity maps for the [Fe II], Paβ, H_2, and Brγ lines over the inner 2.″5 × 0.″75. The slit orientation was east-west, across the two nuclei. The central, brightest knot in both the *J* and *K* bands is identified with the western infrared nucleus and was selected as the reference velocity. The absolute velocity of the Paβ line at the western nucleus was 5380 ± 70 km s^{-1}, and of the Brγ line, 5460 ± 80 km s^{-1}. The mean heliocentric redshift, as determined from CO ($J = 1$–0) emission, is $cz = 5450 \pm 20$ km s^{-1} (Sanders et al. 1988). The fainter knot in the Brγ image is centered 0.″95 ± 0.″08 east of the brighter nucleus and at a relative velocity of +200 ± 25 km s^{-1}. This fainter knot is visible in all four of the individual *K*-band spectra, which rules out its creation through inaccurate chopping or slit curvature. In the Paβ map, significant emission is found coincident with the Brγ knot but is not as centrally concentrated at this second location. The position of this second peak matches that of the eastern infrared nucleus found in the high-resolution *K*-band image of Graham et al. (1990). Figure 2 shows spectra along the eastern and western nuclei, respectively. The lines are essentially unresolved along a single spatial column (a resolution element corresponds to 285 km s^{-1} for the *J* band and 375 km s^{-1} for the *K* band) but appear slightly broadened in Figure 2 because the

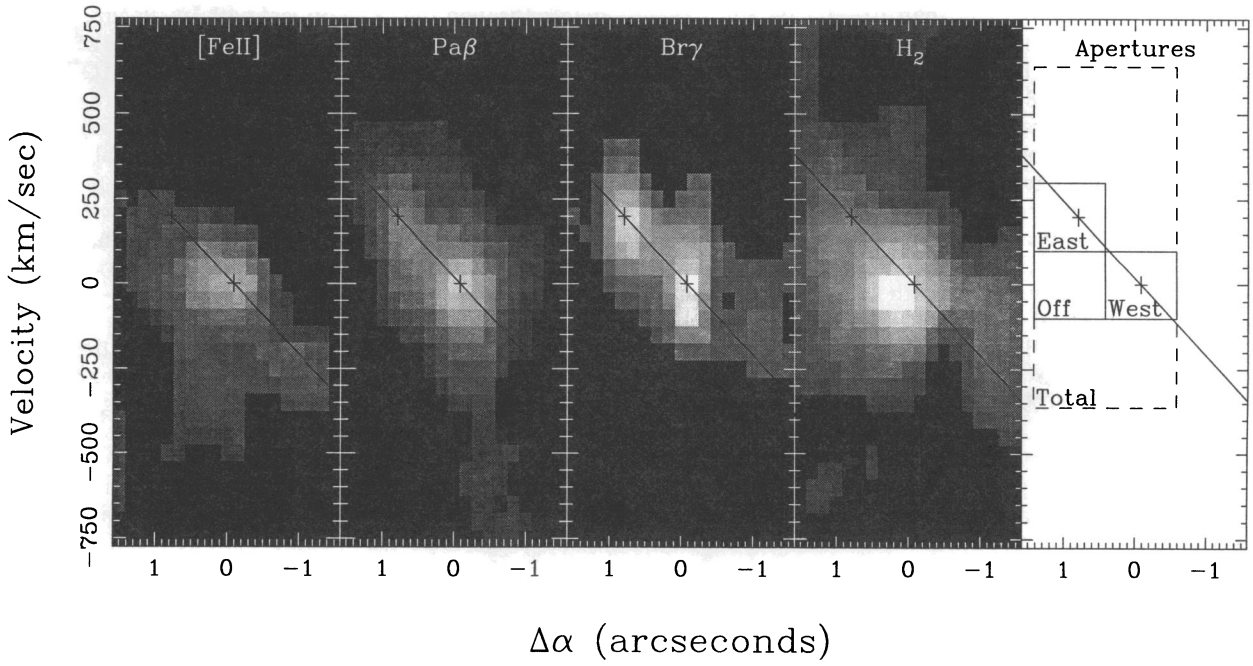

FIG. 1.—[Fe II], Paβ, Brγ, and H_2 position-velocity plots along with a diagram showing the various apertures used to make Table 1. The slit was oriented east-west to include both nuclei which are most visible in the Brγ plot. The western nucleus was selected as the zero-point offset for both axes. Black crosses mark the two Brγ centroids corresponding to the two nuclei, and a straight line is drawn through them to show the velocity gradient. The lowest gray level corresponds to 2.5 σ per resolution element, which was 0.65 times the noise per pixel. The images are plotted from 0 (*black*) to $\frac{2}{3}$ of their peak level (*white*).

© American Astronomical Society • Provided by the NASA Astrophysics Data System

1995ApJ...452..599L

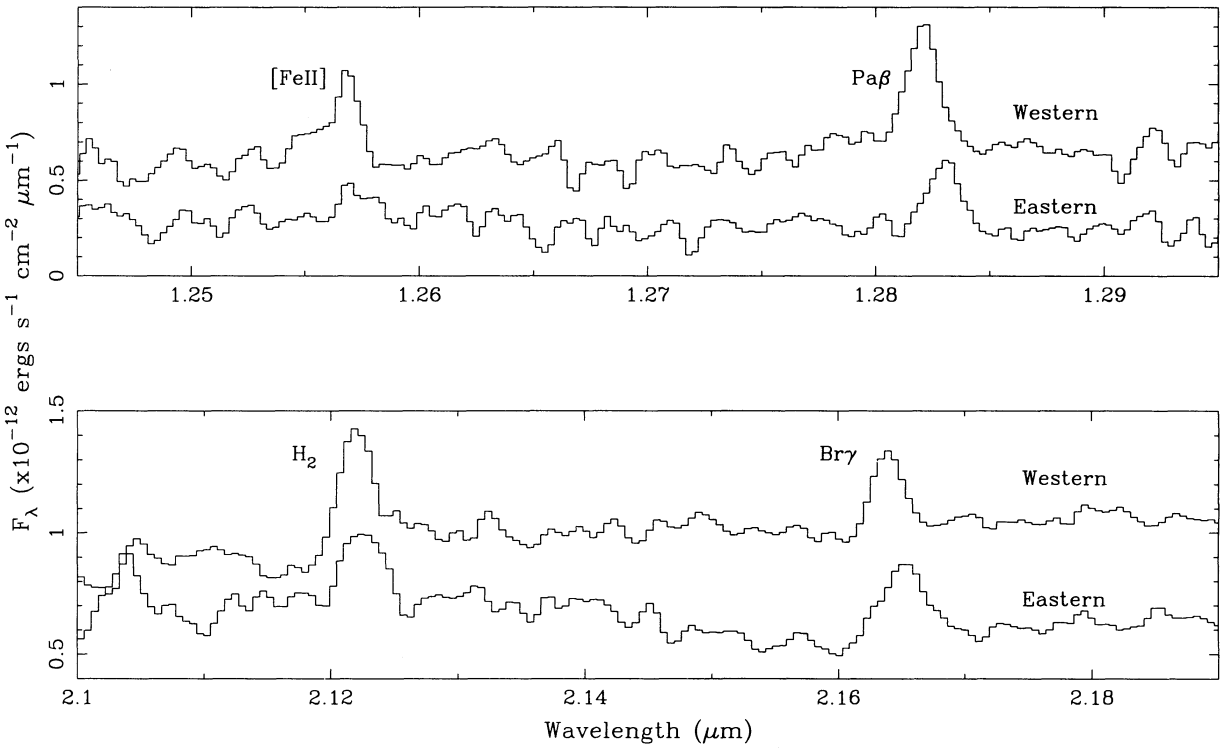

FIG. 2.—*J*- and *K*-band spectra showing all four emission lines discussed in this paper. The spectra represent a synthetic 0.″5 slice centered on the eastern and western nuclei, respectively. The spectra were taken with a 0.″75 slit width with the slit oriented east-west. Note the wavelength shift of the hydrogen recombination lines between the two nuclei. The wavelength scale is given in the rest frame of the western nucleus. The Paβ and Brγ lines appear slightly broadened because the apertures integrate over the observed gradient. The lines are unresolved along an individual spatial pixel column.

apertures integrate over part of the velocity gradient discussed above. The velocity shift found in the hydrogen recombination lines, discussed above, is clearly visible. Through a 5″ diameter aperture, Depoy, Becklin, & Geballe (1987) meaured a Brα (4.05 μm) emission line which they fitted with both one- and two-component Gaussian fits. The two-component fit yielded a "narrow" component with an intrinsic FWHM of 1000 km s^{-1} and a "broad" component with an intrinsic FWHM of 3300 km s^{-1}. We do not see evidence for either of these line components in the Brγ line.

In Table 1, we present the fluxes, line ratios and calculated extinctions for the two nuclei. Four apertures, shown in the last panel of Figure 1, were used on the position-velocity plots to generate this table. First, a 1 × 200 km s^{-1} aperture was placed on the two nuclei, respectively. A similar aperture was also placed at the spatial position of the eastern nucleus but at the velocity of the western nucleus. The last aperture is 2″ × 1000 km s^{-1} and encompasses essentially all of the nuclear emission within our 0.″75 slit. The extinctions are obtained by interpolating the interstellar extinction law of Rieke & Lebofsky (1985) at the rest wavelengths of Paβ and Brγ and using the case B intrinsic line ratio of 0.1647 (Osterbrock 1989). A foreground screen of dust is assumed for the extinction correction. If the dust and emitting sources are mixed, the effective extinction could be much larger. The intrinsic H_2–to–[Fe II] ratio is calculated by correcting the observed ratio for this extinction.

The observation that the Brγ emission is more peaked on the eastern nucleus than the Paβ emission is most easily explained by dust extinction. The calculated extinction at the western nucleus is $A_V \sim 10$ mag compared to $A_V \sim 13$ mag for the eastern nucleus (see Table 1). Both of these numbers are consistent with the small-aperture infrared measurements of Mazzarella et al. (1992) and Armus et al. (1995). Note that the infrared extinctions for each line are interpolated from broadband extinctions given in Rieke & Lebofsky (1985), where $A_J \sim 0.282 A_V$ and $A_K \sim 0.112 A_V$.

3.2. [Fe II] *and* H_2

The measured fluxes for the [Fe II] ($\lambda = 1.2567$ μm) and H_2 ($\lambda = 2.1218$ μm) lines at various locations in the central 2″ are also summarized in Table 1. The flux of the [Fe II] emission in a 2″ × 0.″75 aperture, integrating over all velocities, is somewhat lower than that found in a 2″ × 0.″8 aperture by Armus et al. (1995), being 2.1×10^{-15} ergs s^{-1} cm^{-2} compared to 3.5×10^{-15} ergs s^{-1} cm^{-2}. The Paβ emission, however, which was taken simultaneously with the [Fe II], agrees very well with Armus et al. (1995), being 3.8 versus 4.0×10^{-15} ergs s^{-1} cm^{-2}. A combination of different morphologies in the [Fe II] and Paβ emission lines (the latter is more centrally concentrated) along with slightly improved seeing at the time of the new observations can explain these differences.

An important consideration in the flux calibrations is the accuracy of the stellar flat field at these wavelengths. At the redshift of Arp 220, H_2 is close to the rest wavelength of Brγ, and [Fe II] is close to the rest wavelength of Paβ. The resolution is sufficient to separate possible Balmer contamination in the spectral standard by approximately two-resolution elements from the extragalactic lines. As stated above, we also found no evidence for lines in the spectra of the

© American Astronomical Society • Provided by the NASA Astrophysics Data System

1995ApJ...452..599L

TABLE 1

LINE FLUXES,[a] RATIOS, AND CALCULATED EXTINCTIONS

Quantity	Western Nucleus[b]	Eastern Nucleus[b]	Off Eastern[b,c]	Total Nuclear[d]
Brγ	0.65 ± 0.08	0.53 ± 0.08	0.38 ± 0.08	2.7 ± 0.3
H_2	1.32 ± 0.08	0.76 ± 0.08	1.03 ± 0.08	6.4 ± 0.3
Paβ	1.06 ± 0.05	0.56 ± 0.05	0.45 ± 0.05	3.8 ± 0.2
[Fe II]	0.71 ± 0.05	0.21 ± 0.05	0.40 ± 0.05	2.1 ± 0.2
$\frac{\text{Br}\gamma}{\text{Pa}\beta}$	0.6 ± 0.1	1.0 ± 0.2	0.8 ± 0.3	0.7 ± 0.1
$\frac{H_2}{\text{Br}\gamma}$	2.0 ± 0.4	1.4 ± 0.4	2.7 ± 0.8	2.3 ± 0.3
$\frac{[\text{Fe II}]}{\text{Pa}\beta}$	0.7 ± 0.1	0.4 ± 0.1	0.9 ± 0.2	0.6 ± 0.1
$\frac{H_2}{[\text{Fe II}]}$	1.9 ± 0.2	4 ± 1	2.6 ± 0.5	3.0 ± 0.3
A_V	10 ± 1	13 ± 2	12 ± 2	11 ± 1
$\text{Int}\left(\frac{H_2}{[\text{Fe II}]}\right)^2$	0.5 ± 0.1	0.6 ± 0.3	0.5 ± 0.2	0.6 ± 0.1

[a] Fluxes are in 10^{-15} ergs s^{-1} cm^{-2} and are not corrected for extinction.

[b] Used a 1″ × 200 km s^{-1} aperture. The slit width is 0.″75.

[c] "Off eastern" refers to the position of the eastern nucleus but with the same central velocity as the western nucleus.

[d] A 2″ × 1000 km s^{-1} aperture encompassing essentially all of the nuclear emission in the slit. The slit width is 0.″75.

[e] Intrinsic ratio of H_2/[Fe II] corrected for the extinction calculated from the hydrogen recombination lines as described in the text.

spectral standard. The good agreement in fluxes with Armus et al. (1995) also suggests that the effect is not significant for the current observations.

The [Fe II] and H_2 lines show no significant shift between the two locations, although the H_2 emission is broadened toward higher velocities at the eastern nucleus. The position-velocity plots in Figure 1 show that the H_2 peaks 1.5 pixels (0.″25) to the east of the western nucleus. Such morphological and kinematic differences contribute to the enhanced ratios of [Fe II] and H_2 to the hydrogen recombination lines in the "off eastern" position (Table 1) and the suppression of these ratios on the eastern nucleus. The [Fe II] and H_2 lines are kinematically and spatially distinct from the Paβ and Brγ lines.

4. DISCUSSION

The spectra presented here have separated, both spatially and kinematically, the two nuclei within Arp 220. In the Brγ emission, the nuclei are found to be separated by 0.″95 and 200 km s^{-1}. The Paβ emission shows a similar velocity shift but is not strongly peaked at the location of the eastern nucleus. The centroid of the H_2 emission is not peaked on the western nucleus but is 0.″25 toward the eastern nucleus. The H_2 also does not show the same velocity structure as the hydrogen recombination lines. The [Fe II] emission shows a weak maximum at the location of the western nucleus along with emission in the direction of the eastern nucleus.

An important consideration is how much of the observed velocity shift in the recombination lines could be due to a spatial rotation of the emission-line gas relative to the broad-band emission that was used to position the slit. The recent narrow-band Paβ image by Armus et al. (1995) appears to show a spatial displacement of the Paβ emission that would correspond to a rotation of $<14°$ ($<0.″25$ over 1″ separation). This could contribute up to ~ 95 km s^{-1} to the observed Paβ velocity shift, which would make the actual velocity >105 km s^{-1}. This rotation is quite uncertain, however, since the image has had a very similar continuum image subtracted, and a small alignment error in continuum morphology could generate a fairly large spatial shift. The radio emission peaks (Becklin & Wynn-Williams 1987; Norris 1986) are known to have a position angle of 102°. If the infrared emission had the same angle, it would reduce any observed velocity by ~ 75 km s^{-1}, which would make the actual velocity ~ 275 km s^{-1}. The most likely angle, however, is that of the K-band emission peaks which in Graham et al. (1990) was found to be 92°, which would affect the measured velocity by only 13 km s^{-1}, which makes the actual velocity 213 km s^{-1}. The fact that the observed shift is qualitatively and quantitatively consistent with recent CO millimeter-wave velocities from Scoville et al. (1995) (see below) and the central mass estimates from this velocity shift are consistent with the stellar CO dispersion measurements of Doyon et al. (1994a, b) (see below) gives us confidence that the shift reported here is real, and the uncertainties due to spatial shifts in the nuclei are small. The velocity shift between the western and eastern infrared nuclei in Arp 220 is likely to be close to our measured value of 200 ± 25 km s^{-1}.

The most obvious question is whether the observed kinematic shift is due to the orbital motion of the nuclei. The excellent agreement of the spatial separation of the Brγ peaks with both the 2.2 μm (Graham et al. 1990) and the radio (Becklin & Wynn-Williams 1987; Norris 1988) peaks argues that this shifted emission is closely associated with the nuclei. Recent CO measurements (Scoville et al. 1995) at 1.3 mm reveal a rotational gas motion of ~ 300 km s^{-1} across the central 0.″9 at $\sim 45°$ position angle. Projecting this motion onto our slit (P.A. = 90°) and using our separation of 0.″95 yields a rotation velocity of 220 km s^{-1}. This is very close to the observed Brγ velocity shift of 200 km s^{-1}. Both the spatial agreement with the nuclei and the velocity agreement with the CO rotation rate argue that we are measuring the rotation of the two nuclei. Since Arp 220 has been shown to possess large-scale outflow (Heckman, Armus, & Miley 1987, 1990), it is

© American Astronomical Society • Provided by the NASA Astrophysics Data System

1995ApJ...452..599L

possible, however, that the observed velocity shift may have some component due to nonrotational gas motions along the line of sight.

If the observed velocity shift is predominantly rotational in nature, then we may estimate the nuclear mass. Dynamical friction will circularize the nuclear orbits on a very short timescale. The assumptions that the observed distance and rotation rate are the actual orbital radius and circular velocity and that the orbit is seen edge-on give a lower limit to the nuclear mass. We follow Graham et al. (1990) in assuming that the mass ratio can best be estimated by the K-band flux ratio of 1.6, which, when adjusted for our measured extinctions, becomes 1.2. Although the K-band flux ratio may be affected by supergiants and nonstellar emission processes from the suspected circumnuclear starburst (Rieke et al. 1985), the mass calculation is not extremely sensitive to this ratio unless one of the nuclei completely dominates the mass. In that case the total mass would be twice that calculated below. With these assumptions, the lower nuclear mass limit is $1.5 \pm 0.4 \times 10^9 (H_0/75$ km s^{-1} Mpc^{-1}) $M_\odot$, where the uncertainty is dominated by the uncertainty in the relative velocities. The estimate ignores the possible effects of position angle uncertainty as discussed above. Possible errors in the position angle could reduce our mass calculation by as much as a factor of 4 or increase it by almost a factor of 2. However, we have used the most likely velocity in this calculation, and both the velocity and the derived mass match other estimates from other techniques very well. As an example, the nuclear mass calculated above is very consistent with the value of $1.8 \pm 0.8 \times 10^9$ $M_\odot$ within the central 2″ (Shier, Rieke, & Rieke 1994), estimated from a CO band head (2.3 μm) velocity dispersion of 125 ± 30 km s^{-1} from a preprint of Doyon et al. (1994a). The final quoted velocity dispersion of 150 ± 21 km s^{-1} (Doyon et al. 1994b) would predict a slightly higher value, but it is easily reconciled with our value being a lower mass limit and the uncertainties in the numbers.

The eastern nucleus has a K-band magnitude of 13.7 ± 0.2 mag within a 0.″8 diameter aperture, while the western nucleus is 13.2 ± 0.2 mag (Graham et al. 1990). Using our calculated extinctions of $A_V = 13$ mag and 10 mag on the eastern and western nuclei, respectively, we derive a total nucleur K-band luminosity of 3.3×10^{10} $L_\odot$. This gives an $M/L = 0.05$ within the K band, where we have used +3.41 mag for the absolute K-band magnitude of the Sun (Allen 1973). Most starburst models predict much lower values of M/L (K-band), although the starburst calculations of Leitherer & Heckman (1995) show that extreme models with an aging (10^8 yr) burst can produce an M/L (K-band) of $\sim$0.05. This suggests our estimate of the M/L in the nucleus of Arp 220 is consistent with a starburst only if the burst was isolated in time, occurring $\sim 10^8$ yr ago. The strong CO band absorption seen in the nucleus of Arp 220 (Rieke et al. 1985; Ridgway, Wynn-Williams, & Becklin 1994), however, suggests that young red supergiant stars contribute significantly to the K-band light, implying the age of the starburst is much less than $\sim 10^8$ yr. The large M/L (K-band) we have measured then suggests that a large fraction of the nuclear mass could be tied up in an older preexisting stellar population. The fact that our dynamical mass estimate is only a lower limit would cause us to underestimate M/L and would enhance this effect.

Following Graham et al. (1990), the merging timescale can also be estimated from the rotational velocity using

$$t_m = \frac{2\pi r}{v_c}\left(\frac{M}{m}\right) \quad (1)$$

derived from Binney & Tremaine (1987). Again we take the observed velocity and separation as the circular velocity and orbital radius and a mass ratio of 1.2. This yields a merger time of 1.2×10^7 yr, close to that found by Graham et al. (1990) from an estimated circular velocity of 150 km s^{-1} and a mass ratio of 1.6.

The kinematic differences between the [Fe II] and H_2 compared to the H^+ lines suggest the [Fe II] and H_2 may have an additional excitation source. The extended nature of the [Fe II] and H_2 emission suggests that the nuclei may be surrounded by an extended shocked region. Fast shocks from supernova remnants or from large-scale winds could provide the energy required for this enhancement. Another excitation mechanism could be collisional shocks of interstellar clouds that, because of the ongoing merger process, may still have relative speeds of $\sim$300 km s^{-1}. Since the H_2 centroid lies between the two nuclei and does not follow the hydrogen recombination lines, it may have a strong merger-induced shock component. Similar morphology has been observed in NGC 6240 (van der Werf et al. 1993) and was used to argue that the H_2 emission was excited in shocks from collisions of interstellar material that resulted from an ongoing merger. We cannot, however, at this point discriminate between interstellar cloud collisions and superwind driven shocks. The fact that the H_2/[Fe II] ratio is higher than in most shocked environments may be explained by having some UV excitation of the H_2 by the central ionizing sources. When we take our extinction-corrected Brγ luminosity to derive an ionizing photon luminosity and use the UV fluorescence models in Black & Dishoeck (1987), we find that the UV photon flux is sufficient to power the observed H_2 emission only with the most optimistic models. Most UV fluoresence models fall short by as much as a factor of 100 in generating the observed H_2 emission, which suggests that UV fluorescence is probably not a significant excitation source. Additional observations of other H_2 lines would be useful in discriminating between thermal excitation and UV fluorescence.

The authors would like to thank David Shupe for helpful comments on the paper and assistance with determining instrument sensitivities. We would also like to thank Min Yun and Nick Scoville for useful discussions and access to their recent high-resolution CO map. Thanks also to Eric Becklin for discussions about infrared line widths. Special thanks goes to the telescope assistants at the Hale telescope, Juan Carasco, John Moriarty, and James Hickey, and the entire staff of the Palomar Observatory. Infrared astronomy at Caltech is supported by grants from NASA and NSF. This research has made use of the NASA/IPAC Extragalactic Database (NED) which is operated by the Jet Propulsion Laboratory, Caltech, under contract with NASA.

© American Astronomical Society • Provided by the NASA Astrophysics Data System

1995ApJ...452..599L

REFERENCES

Allen, C. W. 1973, Astrophysical Quantities (London: Athlone)
Armus, L., Shupe, D. L., Matthews, K., Soifer, B. T., & Neugebauer, G. 1995, ApJ, 440, 200
Becklin, E. E., & Wynn-Williams, C. G. 1987, in Star Formation in Galaxies, ed. C. J. Lonsdale (Washington: Government Printing Office), 643
Binney, J., & Tremaine, S. 1987, Galactic Dynamics (Princeton: Princeton Univ. Press)
Black, J. H., & van Dishoeck, E. F. 1987, ApJ, 322, 412
Depoy, D. L., Becklin, E. E., & Geballe, T. R., 1987, ApJ, 316, L63
Doyon, R., Wells, M., Wright, G. S., & Joseph, R. D. 1994a, in Mass Transfer Induced Activity in Galaxies, ed. I. Schlosman (Cambridge: Cambridge Univ. Press), in press
Doyon, R., Wells, M., Wright, G. S., Joseph, R. D., Nadeau, D., & James, R. A. 1994b, ApJ, 437, L23
Graham, J. R., Carico, D. P., Matthews, K., Neugebauer, G., Soifer, B. T., & Wilson, T. D. 1990, ApJ, 354, L5
Heckman, T. M., Armus, L., & Miley, G. K. 1987, AJ, 93, 276
———. 1990, ApJS, 74, 833
Hoffleit, D. 1964, Catalogue of Bright Stars (3d rev. ed.; New Haven: Yale Univ. Obs)
Joseph, R. D., & Wright, G. S. 1985, MNRAS, 214, 87
Joy, M., Lester, D. F., Harvey, P. M., & Frueh, M. 1986, ApJ, 307, 110
Larkin, J. E., Knop, R. A., Lin, S., Matthews, K., & Soifer, B. T. 1995, PASP, submitted
Letherer, C., & Heckman, T. M. 1995, ApJS, 96, 9
Mazzarella, J. M., Soifer, B. T., Graham, J. R., Hafer, C. I., Neugebauer, G., & Matthews, K. 1992, AJ, 103, 413
Neugebauer, G., Elias, J., Matthews, K., McGill, J., Scoville, N., & Soifer, B. T. 1987, AJ, 93, 1057
Norris, R. P. 1988, MNRAS, 230, 345
Oliva, E., & Origha, L. 1992, A&A, 254, 466
Osterbrock, D. E. 1989, Astrophysics of Gaseous Nebulae and Active Galactic Nuclei (Mill Valley: University Science Books)
Ridgway, S. E., Wynn-Williams, C. G., & Becklin, E. E. 1994,ApJ, 428, 609
Rieke, G. H., Cutri, R. M., Black, J. H., Kailey, W. F., McAlary, C. W., Lebofsky, M. J., & Elston, R. 1985, ApJ, 290, 116
Rieke, G. H., & Lebofsky, M. J. 1985, ApJ, 288, 618
Sanders, D. B., Soifer, B. T., Elias, J. H., Madore, B. F., Matthews, K., Neugebauer, G., & Scoville, N. Z. 1988, ApJ, 325, 74
Scoville, N. Z., et al. 1995, in preparation
Shier, L. M., Rieke, M. J., & Rieke, G. H. 1994, ApJ, 433 L9
Soifer, B. T., Sanders, D. B., Madore, B. F., Neugebauer, G., Danielson, G. E., Elias, J. H., Lonsdale, C. J., & Rice, W. L. 1987, ApJ, 320, 238
van der, Werf, P. P., Genzel, R., Krabbe, A., Blietz, M., Lutz, D., Drapatz, S., Ward, M. J., & Forbes, D. A. 1993, ApJ, 405, 522

© American Astronomical Society • Provided by the NASA Astrophysics Data System